

First-principles study on atomic configuration of electron-beam irradiated C_{60} clusters

Tomoya Ono

Graduate School of Engineering, Osaka University, Suita, Osaka 565-0871, Japan

Shigeru Tsukamoto

*Peter Grünberg Institut & Institute for Advanced Simulation,
Forschungszentrum Jülich and JARA, D-52425 Jülich, Germany*

(Dated: January 21, 2013)

Abstract

A theoretical study proposes the atomic configuration of electron-beam irradiated C_{60} thin films. We examined the electronic structure and electron-transport properties of the C_{60} clusters using density-functional calculations and found that a rhombohedral C_{60} polymer with sp^3 -bonded dumbbell-shaped connections at the molecule junction is a semiconductor with a narrow band gap while the polymer changes to exhibit metallic behavior by forming sp^2 -bonded peanut-shaped connections. Conductance below the Fermi level increases and the peak of the conductance spectrum arising from the t_{u1} states of a C_{60} molecule becomes obscure after the connections are rearranged. The present rhombohedral film, including the [2+2] four-membered rings and peanut-shaped connections, is a candidate to represent the structure of the metallic C_{60} polymer at the initial stage of electron-beam irradiation.

PACS numbers: 71.30.+h, 71.15.Mb, 72.80.Rj, 73.61.Wp

I. INTRODUCTION

Intermolecular electron transport has attracted a great deal of attention in numerous fields of research accompanied by the progress in nanostructure-fabrication technology. Fullerene-based molecular crystals and films are of particular interest because of their very rich physical properties such as superconductivity and magnetism. The polymerization of C_{60} molecules in the solid phase using various techniques, e.g., photoirradiation or electron-beam (EB) irradiation, have resulted in new forms of carbon materials.¹ The first-principles study by Okada and Oshiyama reported that the band gap of the rhombohedral phase of the C_{60} polymer linked by [2+2] four-membered rings, where two C atoms shared by the two adjacent hexagons in a C_{60} molecule are covalently bonded to the C atoms shared by the two hexagons in the neighboring C_{60} molecule (e.g., see Fig. 1), is significantly smaller than that of C_{60} bulk.² Onoe *et al.* found that C_{60} films change to polymers accompanying the insulator-metal transition due to EB irradiation and that a one-dimensional (1D) peanut-shaped connection is formed, where C_{60} molecules are linked by sp^2 -like connections instead of sp^3 -like connections,³ and intensive studies on electron transport in the C_{60} polymer have been carried out up to now.⁴ First-principles calculations on the electronic structure of three-dimensional (3D) C_{60} polymers have revealed that 1D peanut-shaped C_{60} polymers are insulators and electrons are conducted across the 1D polymers via [2+2] four-membered rings between the two peanut-shaped C_{60} polymers in the 3D hexagonal structure,^{5,6} which is a completely different configuration from the face-centered cubic structure of C_{60} bulk.

Nakaya *et al.* recently revealed that the chemical linkage between C_{60} molecules created by EB irradiation are thermally more stable than the [2+2] four-membered ring because the polymers are stable under thermal annealing at 220 °C, which is higher than the decomposition temperature of the [2+2] four-membered rings, and they claimed that a peanut-shaped fullerene contributes to the metallic characteristics of EB irradiated film.⁷ They also demonstrated by scanning-tunneling spectroscopy (STS) that the characteristic peak of spectra of the C_{60} molecule disappears at its polymerized center after EB irradiation. Moreover, their scanning tunneling microscopy (STM) images demonstrated that the C_{60} polymers retain a *rhombohedral* structure at the initial stage of EB irradiation; however, this result does not agree with the *hexagonal* structure derived by Onoe *et al.* using first-principles calculations.^{5,6} Thus, the physics underlying the generation of conductivity in EB irradiated

41 C_{60} films remains unclear.

42 In this paper, the atomic configuration of the EB irradiated C_{60} film is proposed by using
43 first-principles calculations. We examine what effect the bond configuration at the molecule
44 junctions has on the electronic structure and electron-transport properties to interpret the
45 generation of conductivity in EB irradiated C_{60} films. Our findings are that the rhombo-
46 hedral C_{60} polymer consisting of the [2+2] four-membered rings and the sp^3 -like interlayer
47 connections create a semiconductor with a narrow band gap and the band gap vanishes
48 when the sp^2 -like interlayer connection is formed. We found significant differences between
49 the conduction spectra of the dimers bonded by the sp^3 -like and sp^2 -like connections; the
50 conductance of the sp^2 -like bonded dimer was higher than that of the sp^3 -like bonded dimer
51 below the Fermi level and the peak of the conductance spectrum caused by the t_{u1} orbitals
52 of the sp^3 -like bonded dimer was clear while that of the sp^2 -like bonded dimer was obscure.

53 All calculations are performed within the framework of density functional theory⁸ using
54 the real-space finite-difference approach, which enables us to determine the self-consistent
55 electronic ground state with a high degree of accuracy by using a timesaving double-grid
56 technique.^{9,10} The norm-conserving pseudopotentials¹¹ of Troullier and Martins¹² are used
57 to describe electron-ion interaction, and exchange correlation effects are treated with local
58 density approximation.¹³

59 II. ELECTRONIC STRUCTURE OF C_{60} POLYMERS

60 C_{60} polymers form a triangular lattice with [2+2] four-membered rings in each poly-
61 merized layer and the layers are stacked along a direction perpendicular to the layers in
62 a rhombohedral symmetry.² When the *ABC*-stacking structure¹⁴ is formed, the layers are
63 bonded by sp^3 -like connections, in which the hexagons on neighboring C_{60} molecules are
64 brought face to face. When the C-C bonds sheared by a hexagon and pentagon on the
65 facing hexagons are distorted, the layers are linked by an sp^2 -like connection consisting
66 of hexagons and heptagons. After this, we will refer to sp^3 -like interlayer connections as
67 dumbbell-shaped and sp^2 -like interlayer connection as peanut-shaped. The peanut-shaped
68 connection is much stronger than the [2+2] four-membered ring because the energy to form
69 it is smaller than that for the [2+2] four-membered ring by 0.02 eV/atom.¹⁵ Therefore, the
70 polymer can be reinforced by the peanut-shaped connection so that it can survive under

71 thermal annealing. We first calculate the electronic structure of the C_{60} polymers.

72 Figure 1 shows two geometries of the models studied here. The C_{60} polymers in model (a)
73 are bonded by the [2+2] four-membered rings in the layer and linked by the dumbbell-shaped
74 connections between the layers. In model (b), one of the dumbbell-shaped connections
75 between the layers is deformed into the peanut-shaped connection. Since the metallic phase
76 of the C_{60} polymer is surrounded by the other phase of the C_{60} s at the initial stage of
77 the EB irradiation according to the STM image,⁷ its lattice parameters are not expected
78 to be fully relaxed. We assume lattice parameters $a=17.37$ bohr, $c=46.30$ bohr and $\alpha =$
79 $\pi/3$, which correspond to those for the dumbbell-shaped interlayer connection obtained
80 by the x-ray diffraction pattern analysis,¹⁶ and employ these lattice parameters for both
81 model (a) and model (b) to compare the contribution of the dumbbell-shaped and peanut-
82 shaped connections to the electronic structures. Note that the stacking structure of the
83 polymer presented in this study is not deformed from the rhombohedral bulk phase and
84 corresponds to the experimentally observed STM image whereas the hexagonal polymers in
85 Refs. 5 and 6 require drastic structural deformation. Integration in the Brillouin zone is
86 carried out using 24-point sampling and structural optimization for the atomic geometris
87 is implemented for both models until the remaining forces for each atom are less than 36
88 meV/bohr. The calculated electronic band structures are depicted in Fig. 2. The energy
89 band gap is reduced by forming peanut-shaped connections; the peanut-shaped polymer
90 exhibits metallic behavior while model (a) is a semiconductor with a fundamental band gap
91 of ~ 0.6 eV. The formation energy of model (b) is larger than that of model (a) by 0.25
92 eV/atom although the formation energy of an isolated peanut-shaped dimer is smaller than
93 that of a dumbbell-shaped dimer by 0.04 eV/atom. Thus, the peanut-shaped connections are
94 not widely generated but C_{60} molecules form small clusters with peanut-shaped connections
95 in the film after EB irradiation.

96 **III. TRANSPORT PROPERTIES OF C_{60} DIMERS**

97 The STS spectra, which have been employed to interpret the transport properties of
98 molecules, show peaks which are distinctly associated with the electronic structure of
99 molecules.¹⁷ However, to replicate the STS spectrum of the C_{60} cluster in the C_{60} film, the
100 system including the large number of atoms are required because a C_{60} molecule contains

60 atoms, which is not easy task by the present computational resources. Moreover, the number of peaks measured for the considered bias-voltage range have been smaller than the number of electronic states in the molecules within the corresponding energy window in some cases.¹⁸ This fact implies that some states of molecules do not contribute to electron transport and that a simple interpretation of transport properties only in terms of DOS is insufficient. In addition, it is well known that the junction between C₆₀ molecules are a bottleneck for electron transport^{19–21} and the energy gap between the highest-occupied molecular orbital (HOMO) and the lowest-unoccupied molecular orbital (LUMO) decreases after polymerization.^{5,6,15,22} One of the present authors (S.T.) examined variations in the local density of states (LDOS) along the 1D C₆₀ polymer axis and demonstrated that the energy gap of LDOS at the molecule junction is larger than that in the C₆₀ molecules.¹⁵ The *sp*²-like connections of the peanut-shaped polymer might enhance electron transport because π electrons are major carriers in metallic carbon nanotubes. Thus, it is of considerable interest to examine how the difference in the bond network between fullerenes contributes to electron transport through fullerenes.

We explore the contribution of the peanut-shaped connection to electron-transport properties. Figure 3 shows the computational model, where a C₆₀ dimer is sandwiched between electrodes. Since the lattice-constant mismatch between the C₆₀ polymers and the electrodes gives rise to further complex discussions on the transport properties, we employ the simplified models to focus on the difference in the contributions to the transport properties between the dumbbell-shaped and peanut-shaped connections. To determine the optimized atomic coordinates and Kohn-Sham effective potential, we use a conventional supercell under a periodic boundary condition in all directions with a real-space grid spacing of ~ 0.32 bohr; the dimensions of the supercell are $L_x = 37.87$ bohr, $L_y = 37.49$ bohr, and $L_z = 71.15$ bohr, where L_x and L_y are the lateral lengths of the supercell in the x - and y -directions parallel to the electrode surfaces, respectively, and L_z is the length in the z direction. Structural optimizations are implemented in advance for the isolated peanut-shaped dimer and it is then placed between the electrodes, where the three topmost surface atomic layers are atomistic Al(111) and the rest are aluminum jellium. The dimer is aligned at the hexagonal-close-packed-hollow site on the (111) surface facing a hexagon, which is the most stable configuration for a C₆₀ molecule on a face centered cubic (111) surface according to first-principles calculations.²³ The distance between the surface atomic layers on the left

and right electrodes is set at 35.81 bohr so that the distance between the edge atoms of the dimer and the surface atomic layer of the electrodes corresponds to that reported by first-principles calculations. The dimer is relaxed between the electrodes. The atomic geometries of 36 carbon atoms for the dumbbell-shaped dimer at the molecule junction are modified from the above mentioned structure and structural optimization is also implemented.

We take a grid spacing of ~ 0.47 a.u for the electron-transport calculations. We ensured that the decreased grid spacing and the enlarged supercell would not significantly affect our results. The scattering wave functions of the electrons propagating from the electrodes are determined by using the method of overbridging boundary matching.^{24–26} The retarded self-energy matrices for aluminum jellium are employed to include the rest of the semi-infinite electrodes. Since the DOS of aluminum is similar to that of free electrons, unfavorable effects from the DOS of the electrodes on the conductance spectra can be eliminated. We first calculate the Kohn-Sham effective potential using the supercell employed in structural optimization and then compute the scattering wave functions obtained non-self-consistently. It has been reported that this procedure is just as accurate in the linear response regime but significantly more efficient than performing computations self-consistently on a scattering-wave basis.²⁷ The conductance of the dimers is described by the Landauer-Büttiker formula, $G = \text{Tr}(\mathbf{T}^\dagger \mathbf{T}) G_0$,²⁸ where \mathbf{T} is a transmission-coefficient matrix.

Figure 4 plots the conductance spectra of the dumbbell-shaped and peanut-shaped dimers as a function of the energy of incident electrons. The magnitude of conductance at the Fermi level and the conduction spectra as a function of the energy of the incident electrons for the dumbbell-shaped dimer are in agreement with those reported in another theoretical study.²¹ Since the dimers are not connected by the [2+2] four-membered rings in a direction parallel to the electrode and the 1D C_{60} polymers act as an insulator, the conductance of the dimers is low around the Fermi level. This implies that the [2+2] four-membered rings play an important role in the metallic characteristics of the C_{60} polymers and the very bright C_{60} molecule in the experimental STM image⁷ is presumably linked by the [2+2] four-membered rings and the peanut-shaped connections as explained in the preceding section. The difference in energy between the peaks of the spectrum around the Fermi level corresponds to the energy gap between the HOMO and the LUMO of the isolated dimers. The peak at $E_F + 0.25$ eV is attributed to the triply degenerate LUMO (t_{u1}) of a C_{60} molecule, where E_F is the Fermi level. The conductance of the peanut-shaped dimer is

165 higher than that of the dumbbell-shaped dimer below the Fermi level and the peak of the
 166 conductance spectrum induced by the t_{u1} orbitals of the dumbbell-shaped dimer is clearer
 167 than that of the peanut-shaped dimer.

168 To examine the contribution of the peanut-shaped connection to the electron-transport
 169 properties in more detail, Fig. 5 shows the LDOS of the dimers, which have been plotted by
 170 integrating them along the plane parallel to the electrode surface, $\rho(z, E) = \int |\psi(\mathbf{r}, E)|^2 d\mathbf{r}_{\parallel}$,
 171 where $\mathbf{r} = (x, y, z)$, ψ is the wave function and E is the energy of the states. The LDOS at
 172 $E_F - 0.2$ eV around the molecule junction of the peanut-shaped dimer is larger than that
 173 of the dumbbell-shaped dimer. The energetically discrete t_{u1} orbitals of the C_{60} molecules
 174 contributing the electron transport change to the broadened states because of the formation
 175 of the sp^2 -like connection at the molecule junction. The states in the electrode can easily
 176 penetrate into the peanut-shaped dimer and the conductance spectrum in Fig. 4 becomes ob-
 177 scure. Although our computational models do not directly correspond to the tip and surface
 178 system of STS, the absence of clear peaks of the t_{u1} orbitals at the center of the polymerized
 179 cluster in the STS spectrum is related to the smooth behavior of the conductance spectrum
 180 induced by the sp^2 -like peanut-shaped connections.

181 IV. SUMMARY

182 The atomic configuration of the EB irradiated C_{60} polymers has been proposed to ex-
 183 plain the generation of the conductivity in the C_{60} film through first-principles calculations.
 184 Although the polymer composed of the [2+2] four-membered rings and dumbbell-shaped
 185 interlayer connections is a semiconductor with a narrow band gap, the polymer changes to
 186 exhibit metallic characteristics by forming a peanut-shaped interlayer connection. The cal-
 187 culations for electron transport for the dumbbell-shaped and peanut-shaped dimers revealed
 188 that the higher conductance of the peanut-shaped dimer below the Fermi level than that of
 189 the dumbbell-shaped dimer and the low peak of the conductance spectrum induced by the
 190 t_{u1} orbitals of the peanut-shaped dimer are relevant to the energetically broadened LDOS at
 191 the molecule junction caused by the formation of the sp^2 -bonded peanut-shaped connection
 192 and the metallic property of the EB-irradiated C_{60} polymer. Rhombohedral film consisting
 193 of [2+2] four-membered rings, dumbbell-shaped and peanut-shaped connections is a possible
 194 structure for the metallic C_{60} polymer observed by STM at the initial stage of EB irradiation.

tion, since the present structure could be formed without significant structural deformation from face-centered cubic C_{60} bulk and agrees with the rhombohedral structure in the STM image. Although our computational models are limited to the simplified C_{60} clusters because of the limitation of the computational resources, the large-scale first-principles calculations for the C_{60} polymers could help to validate the correlation between the STS spectra and the present atomic configuration of the polymers and will be carried out in a future.

ACKNOWLEDGEMENTS

The authors would like to thank Kikuji Hirose and Yoshitada Morikawa of Osaka University for fruitful discussion. This research was partially supported by Strategic Japanese-German Cooperative Program from Japan Science and Technology Agency and Deutsche Forschungsgemeinschaft, by a Grant-in-Aid for Scientific Research on Innovative Areas (Grant No. 22104007) from the Ministry of Education, Culture, Sports, Science and Technology, Japan. The numerical calculation was carried out using the computer facilities of the Institute for Solid State Physics at the University of Tokyo, the Research Center for Computational Science at the National Institute of Natural Science, Center for Computational Sciences at University of Tsukuba, and the Information Synergy Center at Tohoku University.

¹ *Fullerene Polymers and Fullerene Polymer Composites*, edited by P.C. Eklund and A.M. Rao (Springer, Berlin, 2000) and references therein.

² S. Okada and A. Oshiyama, Phys. Rev. B **68**, 235402 (2003).

³ J. Onoe, T. Nakayama, M. Aono, and T. Hara, Appl. Phys. Lett. **82**, 595 (2003).

⁴ See, e.g., J. Onoe, A. Takashima, and Y. Toda, Appl. Phys. Lett. **97**, 241911 (2010).

⁵ S. Ueda, K. Ohno, Y. Noguchi, S. Ishii, and J. Onoe, J. Phys. Chem. B **110**, 22374 (2006).

⁶ J. Onoe, T. Ito, S.I. Kimura, K. Ohno, Y. Noguchi, and S. Ueda, Phys. Rev. B **75**, 233410 (2007).

⁷ M. Nakaya, M. Aono, and T. Nakayama, Carbon **49**, 1829 (2011).

⁸ P. Hohenberg and W. Kohn, Phys. Rev. **136**, B864 (1964).

- ⁹ K. Hirose, T. Ono, Y. Fujimoto, and S. Tsukamoto, *First Principles Calculations in Real-Space Formalism, Electronic Configurations and Transport Properties of Nanostructures* (Imperial College, London, 2005).
- ¹⁰ T. Ono and K. Hirose, Phys. Rev. Lett. **82**, 5016 (1999); Phys. Rev. B **72**, 085115 (2005); T. Ono, M. Heide, N. Atodiresei, P. Baumeister, S. Tsukamoto, and S. Blügel, Phys. Rev. B **82**, 205115 (2010).
- ¹¹ We used the norm-conserving pseudopotentials NCPS97 constructed by K. Kobayashi. See K. Kobayashi, Comput. Mater. Sci. **14**, 72 (1999).
- ¹² N. Troullier and J. L. Martins, Phys. Rev. B **43**, 1993 (1991).
- ¹³ J. P. Perdew and A. Zunger, Phys. Rev. B **23**, 5048 (1981).
- ¹⁴ X. Chen, S. Yamanaka, K. Sako, Y. Inoue, and M. Yasukawa, Chem. Phys. Lett. **356**, 291 (2002).
- ¹⁵ S. Tsukamoto and T. Nakayama, J. Chem. Phys. **122**, 074702 (2005).
- ¹⁶ M. Núñez-Regueiro, L. Marques, J.-L. Hodeau, O. Béthoux, and M. Perroux, Phys. Rev. Lett. **74**, 278 (1995).
- ¹⁷ J. Tersoff and D.R. Hamann, Phys. Rev. B **31**, 805 (1985).
- ¹⁸ H. Hövel, B. Grimm, M. Bödecker, K. Fieger, and B. Reihl, Surf. Sci. **463**, L603 (2000); H. Hövel and I. Barke, Prog. Surf. Sci. **81**, 53 (2006); M. De Menech, U. Saalman, and M.E. Garcia, New J. Phys. **9**, 340 (2007).
- ¹⁹ M. Otani, T. Ono, and K. Hirose, Phys. Rev. B **69**, 121408(R) (2004).
- ²⁰ T. Ono and K. Hirose, Phys. Rev. Lett. **98**, 026804 (2007).
- ²¹ G. Schull, T. Frederiksen, M. Brandbyge, and R. Berndt, Phys. Rev. Lett. **103**, 206803 (2009).
- ²² H. Nakayama, T. Ono, H. Goto, and K. Hirose, Sci. Tech. Adv. Mater. **8**, 196 (2007).
- ²³ L.-L. Wang and H.-P. Cheng, Phys. Rev. B **69**, 165417 (2004).
- ²⁴ Y. Fujimoto and K. Hirose, Phys. Rev. B **67**, 195315 (2003).
- ²⁵ L. Kong, M.L. Tiago, and J.R. Chelikowsky, Phys. Rev. B **73**, 195118 (2006).
- ²⁶ Y. Egami, K. Hirose, and T. Ono, Phys. Rev. E **82**, 056706 (2010).
- ²⁷ L. Kong, J.R. Chelikowsky, J.B. Neaton, and S.G. Louie, Phys. Rev. B **76**, 235422 (2007).
- ²⁸ M. Büttiker, Y. Imry, R. Landauer, and S. Pinhas, Phys. Rev. B **31**, 6207 (1985).

251

FIGURES

252

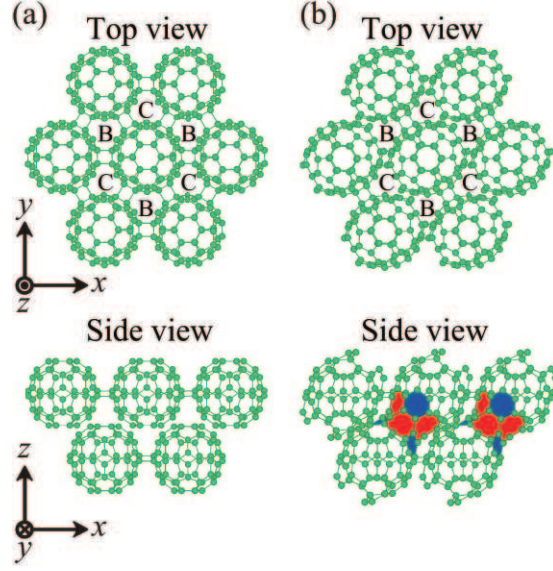


FIG. 1. (color online) Geometric structure of 3D C_{60} polymer phases. (a) Polymer bonded by only $[2+2]$ four-membered rings and dumbbell-shaped connections and (b) polymer in which one of three dumbbell-shaped connections deforms to the peanut-shaped connection. The shaded segments in (b) represent the hexagons (blue) and heptagons (red) of the peanut-shaped connection. B and C in the top views correspond to the positions of C_{60} molecules in the upper and lower layers.

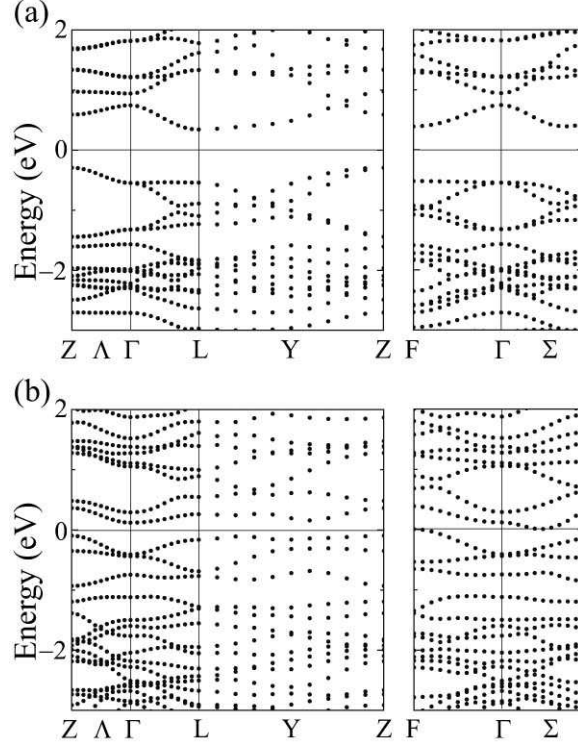


FIG. 2. Band structures of 3D C₆₀ polymers of models (a) and (b) in Fig. 1. Zero energy was chosen as the Fermi level.

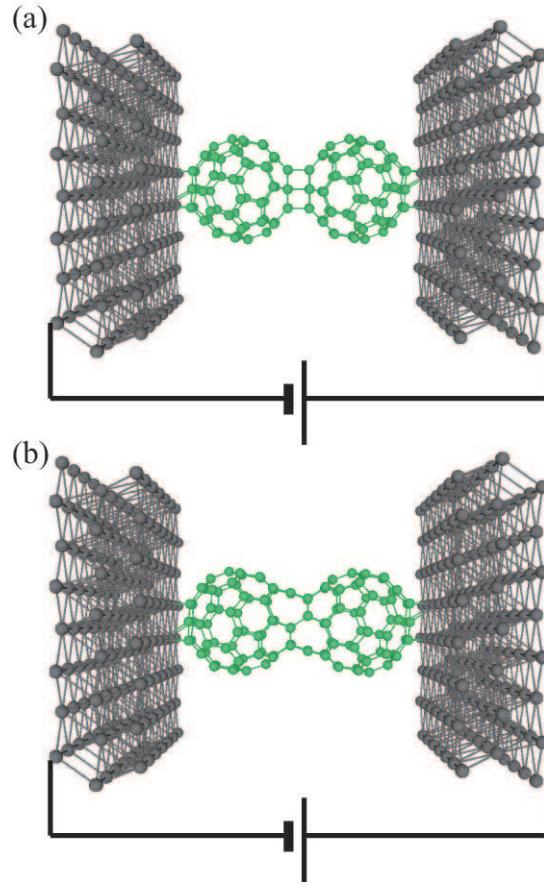


FIG. 3. (color online) Computational model where C_{60} dimer is suspended between Al(111) electrodes. (a) Dumbbell-shaped dimer and (b) peanut-shaped dimer.

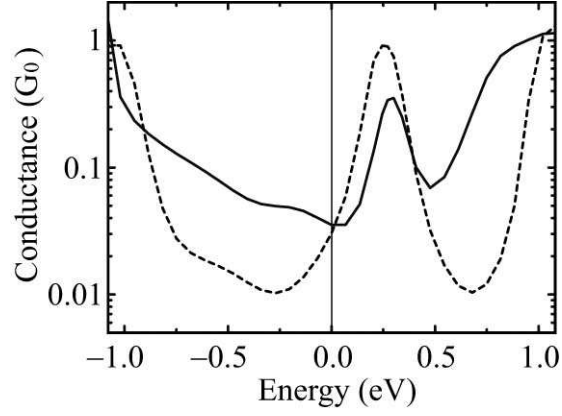


FIG. 4. Conductance spectra as function of energy of incident electrons. The dashed curve represents the conductance of the dumbbell-shaped dimer and the solid curve that of the peanut-shaped dimer. Zero energy was chosen as the Fermi level.

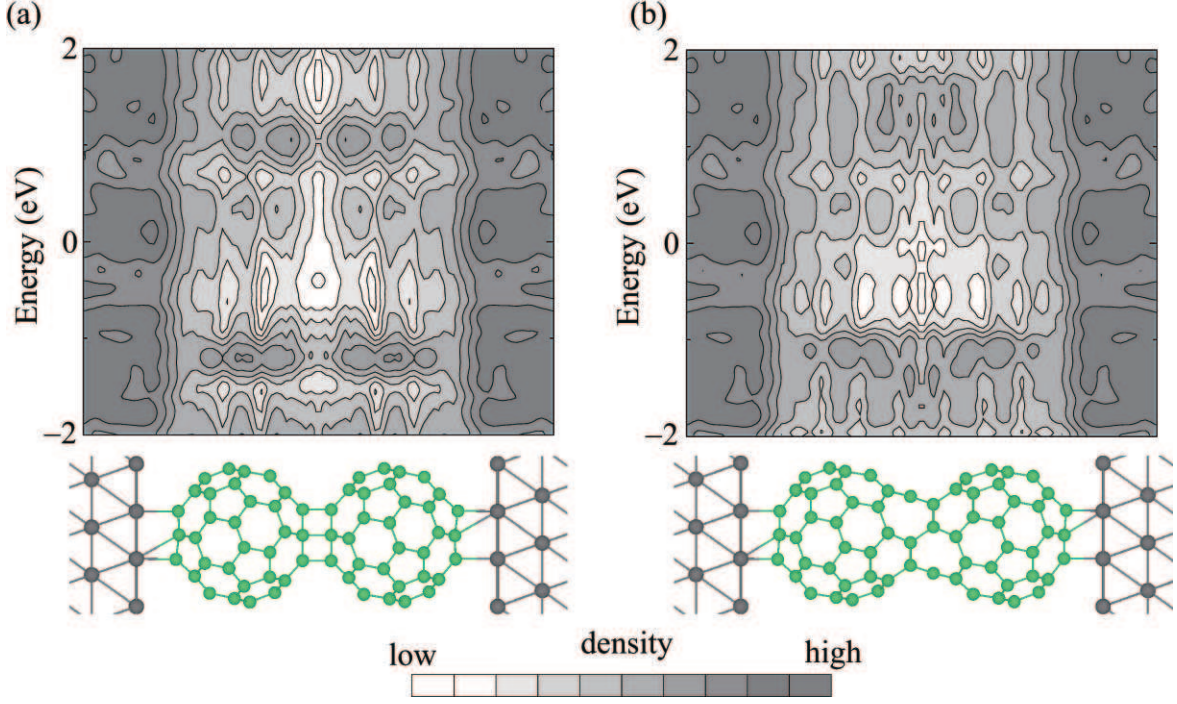


FIG. 5. (color online) Distributions of LDOS integrated on plane parallel to dimer as functions of relative energy from Fermi level. Zero energy is chosen as the Fermi level. Each contour represents twice or half the density of the adjacent contour lines, and the lowest contour is 2.56×10^{-4} $e/eV/\text{bohr}$. The atomic configurations below the graph are visual guides.